SLAC – PUB – 3820
DESY 85 – 019
October 1985
(E)

THE χ_b STATES IN EXCLUSIVE RADIATIVE DECAY OF THE $\Upsilon(2S)$ *

W. Walk[j], P. Zschorsch[e], D. Antreasyan[i], D. Aschman[b], D. Besset[k], J.K. Bienlein[e], E.D. Bloom[l], I. Brock[c], R. Cabenda[k], A. Cartacci[g], M. Cavalli-Sforza[k‖] R. Clare[l], G. Conforto[g], S. Cooper[l], R. Cowan[k‖], D. Coyne[k‖], C. Edwards[a], A. Engler[c], G. Folger[f], A. Fridman[l†] J. Gaiser[l], D. Gelphman[l‖], G. Godfrey[l], F.H. Heimlich[h], R. Hofstadter[l], J. Irion[i], Z. Jakubowski[d], S. Keh[m], H. Kilian[m], I. Kirkbride[l], T. Kloiber[e], W. Koch[e], A.C. König[j], K. Königsmann[m], R.W. Kraemer[c], R. Lee[l‖], S. Leffler[l], R. Lekebusch[h], P. Lezoch[h], A.M. Litke[l‖], W. Lockman[l‖], S. Lowe[l], B. Lurz[f], D. Marlow[c*], W. Maschmann[h], T. Matsui[l•], F. Messing[c], W.J. Metzger[j], B. Monteleoni[g], R. Nernst[h], C. Newman-Holmes[k‡], B. Niczyporuk[l%], G. Nowak[d], C. Peck[a], P.G. Pelfer[g], B. Pollock[l], F.C. Porter[a], D. Prindle[c◇], P. Ratoff[a‡], B. Renger[c], C. Rippich[c], M. Scheer[m], P. Schmitt[m], M. Schmitz[e], J. Schotanus[j], A. Schwarz[l‖], D. Sievers[h], T. Skwarnicki[e%], K. Strauch[i], U. Strohbusch[h], J. Tompkins[l], H.J. Trost[e♭], R.T. Van de Walle[j], H. Vogel[c], U. Volland[f], K. Wacker[l‡], H. Wegener[f], D. Williams[i]

THE CRYSTAL BALL COLLABORATION

[a] *California Institute of Technology, Pasadena, CA 91125*
[b] *University of Cape Town, Cape Town, South Africa*
[c] *Carnegie-Mellon University, Pittsburgh, PA 15213*
[d] *Cracow Institute of Nuclear Physics, Cracow, Poland*
[e] *Deutsches Elektronen Synchrotron DESY, Hamburg, Germany*
[f] *Universität Erlangen-Nürnberg, Erlangen, Germany*
[g] *INFN and University of Firenze, Italy*
[h] *Universität Hamburg, I. Institut für Experimentalphysik, Hamburg, Germany*
[i] *Harvard University, Cambridge, MA 02138*
[j] *University of Nijmegen and NIKHEF-Nijmegen, The Netherlands*
[k] *Princeton University, Princeton, NJ 08544*
[l] *Department of Physics, HEPL, and Stanford Linear Accelerator Center, Stanford University, Stanford, CA 94305*
[m] *Universität Würzburg, Würzburg, Germany*

Submitted to *Physical Review D*

* Work supported in part by the Department of Energy, contracts DE-AC03-81ER40050 (CIT), DE-AC02-76ER03066 (CMU), DE-AC02-76ER03064 (Harvard), DE-AC02-76ER03072 (Princeton), DE-AC03-76SF00515 (SLAC), DE-AC03-76SF00326 (Stanford), and by the National Science Foundation, Grants PHY75-22980 (CIT), PHY81-07396 (HEPL), PHY82-08761 (Princeton).

ABSTRACT

The Crystal Ball detector at DORIS II has been used to study radiative decays of the $\Upsilon(2S)$ resonance. We report on the analysis of the exclusive channel $\Upsilon(2S) \rightarrow \gamma\chi_b$, $\chi_b \rightarrow \gamma\Upsilon(1S) \rightarrow e^+e^-$or $\mu^+\mu^-$. We detect two χ_b states by observing two monochromatic photon lines at energies $(107.0 \pm 1.1 \pm 1.3)$ MeV and $(131.7 \pm 0.9 \pm 1.3)$ MeV respectively. The product branching ratios $\mathrm{BR}\left[\Upsilon(2S) \rightarrow \gamma\chi_b\right] \times \mathrm{BR}\left[\chi_b \rightarrow \gamma\Upsilon(1S)\right]$ are $(1.6 \pm 0.3 \pm 0.2)\%$ for the first state and $(2.1 \pm 0.3 \pm 0.3)\%$ for the second. For the product branching ratio of the third χ_b state, which has been observed in inclusive measurements, we find an upper limit of 0.2% (90% C.L.). Combining our results with inclusive measurements, branching ratios for $\chi_b \rightarrow \gamma\Upsilon(1S)$ are derived. Using theoretical estimates for the radiative widths of the χ_b states, we determine their hadronic widths; the results are compared with QCD predictions.

I. Introduction

In this paper we report the results of a study of the radiative transitions from the $\Upsilon(2S)$ to the $\Upsilon(1S)$ via the χ_b states. Mesons of the Υ family are well described as $b\bar{b}$ quark pairs bound in a central potential [1]. In contrast to lighter $q\bar{q}$ systems, composed of u, d, s, or c quarks, relativistic kinematic effects are smaller when calculating the radiative transitions among the Υ bound states. Figure 1 shows the energy levels of the $\Upsilon(1S)$ and $\Upsilon(2S)$ as well as the states that can be reached from the latter by radiative transitions; the solid lines represent the radiative transitions which have been experimentally observed[2–5]. The three $\Upsilon(2S) \to \chi_b^J \left[\chi_b^J \equiv 1^3P_J\right]$ photon transitions were only recently resolved[4–5].

One approach to studying the radiative transitions is the observation of monochromatic lines in the inclusive photon spectrum associated with decay events taken on the $\Upsilon(2S)$ resonance. A complementary technique uses the cascade sequence

$$\begin{array}{l} \Upsilon(2S) \to \gamma\chi_b \\ \qquad\quad \big\lfloor\!\!\longrightarrow \gamma\Upsilon(1S) \\ \qquad\qquad\quad \big\lfloor\!\!\longrightarrow e^+e^- \text{ or } \mu^+\mu^- \ . \end{array} \tag{1}$$

The latter, which is the subject of this paper, provides a largely background-free method for identifying the χ_b states and studying their properties.

Our analysis is based on $(201 \pm 16) \times 10^3$ $\Upsilon(2S)$ decays observed with the Crystal Ball detector at the DORIS II e^+e^- storage ring at DESY. The data sample corresponds to an integrated luminosity of 63.1 pb^{-1}.

In section II we discuss the technical features of the Crystal Ball detector relevant to the analysis presented here; a more detailed description has been presented elsewhere[6]. In section III the event selection leading to the final event sample is described. In section IV we present our results and compare them with Crystal Ball inclusive photon measurements and with previous cascade results[3]. In section V our results are compared with QCD predictions. Section VI is reserved for conclusions.

II. The Detector

The Crystal Ball apparatus, shown in Fig. 2, is a non-magnetic detector designed for measuring electromagnetically showering particles. The excellent energy and angular resolution of the Ball, resulting from its depth of 16 radiation lengths and its high segmentation, make it well suited to study $\gamma\gamma e^+e^-$ and $\gamma\gamma\mu^+\mu^-$ final states. Its major component is a spherical shell of 672 tapered NaI(Tl) crystals, covering 93% of the total solid angle. Two arrays of endcap crystals increase the coverage of the solid angle to 98%.

The energy resolution for electromagnetically showering particles is[6-8]

$$\sigma(E)/E = (2.7 \pm 0.2 \pm 0.2)\%/\sqrt[4]{E(\mathrm{GeV})} \quad . \tag{2}$$

A typical shower is distributed over approximately 13 crystals. Using an algorithm to find the center of a shower, an angular resolution of 1° to 2° is achieved, depending on the energy. The energy response of the NaI(Tl) crystals to a monochromatic electromagnetic particle is slightly asymmetric but well fitted by the sum of a Gaussian combined with a polynomial tail toward lower energies[7]. The parameters of this so-called NaI-line shape function were fixed in previous studies of the reaction $\psi(2S) \to \eta J/\psi$, $\eta \to \gamma\gamma$ [8]. Unlike photons and electrons, high energy muons do not deposit all their energy in the crystals. Their energy deposition follows a Landau spectrum peaking at 210 MeV, the most probable energy loss for a minimum ionizing particle crossing 16 radiation lengths of NaI. This energy is deposited in one or two crystals only; thus, the angular resolution for minimum ionizing particles is 2° to 3°. Typical energy patterns for muons, electrons and photons are shown in Figs. 3 and 4, which present Mercator-type crystal projections of the Ball, each showing a cascade event candidate.

Three double layers of proportional tube chambers with charge division readout are used to identify charged particles. Electrons are recognized by their large energy deposition in the crystals and the presence of an associated track in the tube chambers. Muons are identified by a chamber track pointing to a minimum ionizing energy pattern in the NaI(Tl). Photons are seen as particles with a

typical electromagnetic shower pattern, but without an associated track in the chambers.

The NaI(Tl) energy scale is fixed by measuring large angle Bhabha events. The time stability of the electronics associated with each channel was checked using a light flasher system. Studies of the $\Upsilon(2S) \to \pi^0\pi^0\Upsilon(1S)$ decay channel, show that a linear relation between the measured pulse height and the energy deposition in the crystals leaves both the π^0 mass and the mass difference $\Delta M = M[\Upsilon(2S)] - M[\Upsilon(1S)]$ about 5% below the established values[9-10]. We therefore correct our energy calibration with a one-parameter non-linear expression found to work well for photons in the 50 to 300 MeV region of the channel $\Upsilon(2S) \to \pi^0\pi^0\Upsilon(1S) \to \gamma\gamma\gamma\gamma\Upsilon(1S)$

$$E_{corr} = \frac{E_{meas}}{1 + \alpha \ln (E_{meas}/E_{beam})} \tag{3}$$

with $\alpha = 0.0137$; the value of α was derived from a fit making both the η^0 mass and the $2S$-$1S$ mass-difference agree with their nominal values.

III. Event Selection

For trigger and selection purposes we use the "Main Ball", *i.e.*, all crystals which are not in the so-called tunnel regions (two layers of 30 crystals closest to the beam entrances).

The triggers relevant to this analysis were:

(a) A total energy trigger, which requires the total energy deposited in the Main Ball to exceed 1700 MeV.

(b) A topology trigger, which requires the total energy in the Main Ball to be above 760 MeV and to be roughly symmetrically deposited around the interaction point. The latter condition is implemented by dividing the Main Ball in (ten) different ways into two hemispheres and requiring for each of these configurations to have at least 150 MeV energy deposited in each hemisphere.

(c) A "μ-pair" trigger, which requires more than 220 MeV in the Main Ball, two back-to-back energy clusters and less than 40 MeV in each tunnel region. Clusters are considered back-to-back if the directions of their centers are acolinear by less than 40°.

The total energy trigger is expected to detect all $\gamma\gamma e^+e^-$ events within the accessible solid angle, while the topology trigger and the μ-pair trigger are intended to detect the $\gamma\gamma\mu^+\mu^-$ events which only deposit about 950 MeV. The efficiencies of all three triggers are determined using Monte Carlo simulated cascade events surviving the software selection. The results obtained vary by approximately 1% depending on the spin assumption used. Averaged over all possible spin hypotheses, one finds for the $\gamma\gamma e^+e^-$ cascades efficiencies of $\sim$ 100%, $\sim$ 99% and $\sim$ 100% for the total energy, topology and μ-pair trigger respectively; for the $\gamma\gamma\mu^+\mu^-$ cascades the corresponding numbers are $\sim$ 0%, $\sim$ 94% and $\sim$ 93%. The combined efficiency of all three triggers is larger than 98% for all μ-channel cascades events and nearly 100% for all e-channel cascades.

To search for events of the cascade type [Eq. (1)], all such triggered events are subjected to a set of criteria optimized for selecting the characteristic topology involved, namely two almost back-to-back leptons and two additional photons. The software selection is carried out as follows:

(i) An event must have exactly four particles (energy clusters larger than 10 MeV) in the Main Ball and no particles in the tunnel region.

(ii) There must be two particles (the lepton candidates) with an electron signature, or two particles with a muon signature from the crystals. We require that at least one of the lepton candidates has an associated charged track in the tube chambers. In addition, the opening angle of the lepton candidates must be greater than 160°.

(iii) The two remaining particles must each have an energy of at least 50 MeV and have a photon signature. This 50 MeV cut eliminates background, but also limits the accessible photon energy range.

(iv) To provide a good energy measurement, each particle is required to deposit its energy in an isolated group of crystals. This is achieved by applying a cut on the opening angle, α, between each pair of particles of such that $\cos\alpha < 0.8$, if both particles are showering, or $\cos\alpha < 0.9$, if one is minimum ionizing.

(v) To eliminate background in the $\gamma\gamma\mu^+\mu^-$ channel, both the unassociated energy (not belonging to any of the particles) in the Main Ball and the energy deposited in the endcaps are required to be less than 45 MeV.

(vi) Finally, all events must pass a two-constraint kinematic fit, using energy and momentum conservation, to the hypothesis $\gamma\gamma l^+l^-$. The lepton energies and the intermediate χ_b and $\Upsilon(1S)$ mass constraints are not used in the fit.

After imposing all the above cuts we are left with a sample of 282 $\gamma\gamma l^+l^-$ events.

IV. Results

1. The energy levels of the χ_b states.

Figure 5 shows a scatter plot of $E_{\gamma low}$ (defined as the lowest of the two photon energies) *vs.* the mass difference $\Delta M = M[\Upsilon(2S)] - M[l^+l^-]$ for all events surviving the selection procedure described in section III. $M(l^+l^-)$ is the effective mass of the two leptons recoiling against the photons; it is calculated using the $\Upsilon(2S)$-mass[11] and the measured four-momentum vectors of the two photons; the fact that the $\Upsilon(2S)$ decaying into two leptons is always close to being at rest implies that given the resolution of our detector, using the angles of the charged lepton tracks in fitting $M(l^+l^-)$ yields no improvement. Two distinct $E_{\gamma low}$ clusters are observed in the region of $\Delta M \sim 560$ MeV.

Figure 6 shows the projection of the scatter plot on the ΔM axis for 440 MeV$< \Delta M <$ 680 MeV; the peaking of events in the region of the $\Upsilon(2S) - \Upsilon(1S)$ mass difference indicates that we indeed see the photon transitions from the $\Upsilon(2S)$ to

the $\Upsilon(1S)$. A fit to this distribution using a NaI-line shape (see section II) on top of a flat background gives $\Delta M_{peak} = (562 \pm 2)$ MeV, in good agreement with the precise mass difference measurement[10], and a width consistent with our experimental resolution ($\sigma = (16 \pm 2)$ MeV). The ΔM distribution is used to apply a final cut to the data; all events outside $\Delta M_{peak} \pm 3\sigma$ are eliminated. Monte Carlo studies show that this (symmetric) cut eliminates about 3% of 'good' events at the low-end side of the ΔM-distribution and less than 1% at the high-end side, the asymmetry originating from the non-Gaussian nature of the NaI-energy response. After this cut a sample of 58 $\gamma\gamma e^+e^-$ decays and 42 $\gamma\gamma\mu^+\mu^-$ decays remains.

The projection of this final sample on the $E_{\gamma low}$ axis is shown in Fig. 7. This distribution shows two well-separated peaks at about 107 MeV and 132 MeV respectively, with widths consistent with our experimental resolution. Our data do not show an indication of a third $\Upsilon(2S) \rightarrow \gamma\chi_b$ transition, which was seen in inclusive analyses[4-5] at about 164 MeV. In the following we will assume that the 107 MeV line corresponds to the decay $\Upsilon(2S) \rightarrow \gamma\chi_b^2$ and the 132 MeV line to the decay $\Upsilon(2S) \rightarrow \gamma\chi_b^1$. This agrees with expectations from potential model calculations and with our preliminary spin determination of these states[12]. This assumption is also consistent with the theoretical prediction that the transition $\chi_b^0 \rightarrow \gamma\Upsilon(1S)$ has a smaller branching ratio than the other two transitions[13].

A fit to the distribution of Fig. 7 in the region 50 to 200 MeV, using two NaI-line shapes with widths fixed to our energy resolution [Eq. (2)] on top of a flat background, yields the following energies, E_J,

$$\begin{aligned} E_2 &= (107.0 \pm 1.1 \pm 1.3) \text{ MeV} \quad , \\ E_1 &= (131.7 \pm 0.9 \pm 1.3) \text{ MeV} \quad , \end{aligned} \tag{4}$$

where the first error is statistical and the second systematic.

Fitting the $\gamma\gamma e^+e^-$ and $\gamma\gamma\mu^+\mu^-$ channels separately yields compatible values as shown by the results displayed in Table 1. Estimates of the systematic errors from energy scale uncertainty, event selection and fitting procedure are listed in

Table 2. The final error was obtained by continuing the sub-errors linearly, rather than in quadrature. Linear addition of the errors was chosen after comparing the energies of the two χ_b lines as measured in both exclusive and inclusive analyses. For the bottomonium system (this paper) and also charmonium (see Refs. 6 and 7) the Crystal Ball Collaboration measured the two lines by these two different methods. If we add the separate sources of systematic errors linearly all corresponding measurements agree within one standard deviation. In three out of four cases, adding the errors in quadrature did not give agreement between the corresponding measurements within one standard deviation. This apparent inconsistency may indicate an unknown source of systematic error.

Both line energies agree within error with the CUSB cascade results[3] of $(107^{+2.5}_{-2.0})$ MeV for E_2 and (128 ± 1.5) MeV for E_1 (the CUSB results have an additional scale error of about 2 MeV). The E_2 and E_1 values agree within error with the corresponding energies determined from our inclusive spectrum[4] of $(110.4 \pm 0.8 \pm 2.2)$ MeV and $(130.6 \pm 0.8 \pm 2.4)$ MeV respectively. Combining the values [Eq. (4)] with the corresponding inclusive results, we obtain the following weighted averages, E_J^{av},

$$\begin{aligned} E_2^{av} &= (108.2 \pm 1.6) \text{ MeV} \quad , \\ E_1^{av} &= (131.4 \pm 1.5) \text{ MeV} \quad . \end{aligned} \tag{5}$$

To calculate the weights for the average, the contribution from the uncertainty in the energy scale has been taken out, as this is common to both the exclusive and inclusive analysis. In the final error quoted, however, this source is again added in linearly. The remainder of the systematic errors and the statistical errors are combined in quadrature.

For the energy difference $\Delta E \equiv E_1 - E_2$ the systematic error due to the energy scale is reduced to 0.1 MeV. We find

$$\Delta E_{excl} = (24.7 \pm 1.7) \text{ MeV} \quad . \tag{6}$$

The value obtained from the inclusive analysis is $\Delta E_{incl} = (20.2 \pm 1.8)$ MeV.

The difference between these two measurements of the same splitting is less than 2 standard deviations.

Defining M_J as the mass of the χ_b^J state we obtain from the averaged photon energies [Eq. (5)],

$$\begin{aligned} M_2 &= (9914.6 \pm 1.6)\ \text{MeV} \ , \\ M_1 &= (9891.1 \pm 1.5)\ \text{MeV} \ , \end{aligned} \tag{7}$$

where we assume $M[\Upsilon(2S)] = (10023.4 \pm 0.3)$ MeV[11]. Using [Eq. (7)], and $M_0 = (9858.2 \pm 3.1)$ MeV from our inclusive analysis[4], we calculate the center of gravity for the χ_b states, $M\left[\chi_b^{cog}\right] \equiv \sum_J (M_J\,[2J+1]) / \sum_J (2J+1)$, to be

$$M\left[\chi_b^{cog}\right] = (9900.5 \pm 1.3)\ \text{MeV} \ . \tag{8}$$

In Table 3 we compare our value for $M\left[\chi_b^{cog}\right]$ with predictions from several models. The recent predictions from the model of Ref. 20 agrees best with our measurement. We also give in Table 3 the ratio $r \equiv [M_2 - M_1] / [M_1 - M_0]$, which parametrizes the fine structure splitting. In this case our result is in good agreement with the predictions of the models of Refs. 14, 15 and 17. The precise measurements of the radiative transitions now available should help to improve the theoretical description of quarkonium features.

2. Branching Ratios:

The product branching ratio

$$\begin{aligned} \text{BR}_J\left[\Upsilon(2S) \to \gamma\gamma l^+ l^-\right] \equiv \text{BR}\left[\Upsilon(2S) \to \gamma\chi_b^J\right] \times \text{BR}\left[\chi_b^J \to \gamma\Upsilon(1S)\right] \\ \times\ \text{BR}\left[\Upsilon(1S) \to l^+ l^-\right] \end{aligned} \tag{9}$$

for the three step decay chain of [Eq. (1)] can be calculated from

$$\text{BR}_J\left[\Upsilon(2S) \to \gamma\gamma l^+ l^-\right] = \frac{N_J(\gamma\gamma l^+ l^-)}{N_{res}\left[\Upsilon(2S)\right] \times \epsilon_J(\gamma\gamma l^+ l^-)} \ , \tag{10}$$

where N_J is the number of observed $\gamma\gamma l^+l^-$ events in the χ_b^J channel surviving all selection criteria, ϵ_J is the detection efficiency and $N_{res}\,[\Upsilon(2S)]$ is the total number of produced $\Upsilon(2S)$ decays.

The numbers of events N_2 and N_1, obtained from separate fits of the $(\gamma\gamma e^+e^-)$ and $(\gamma\gamma\mu^+\mu^-)$ distributions, are listed in Table 1. The number of background events obtained from the fits and the background estimates from the population of the sidebands (see Fig. 5) are also presented; the two values agree within errors. There are several processes that may contribute to the background. Below we give estimates of these processes in the photon energy range of interest *i.e.*, between $E_2 - 3\sigma_2$ and $E_1 + 3\sigma_1$ (or from about 93 MeV to about 148 MeV), where σ_2 and σ_1 are the widths fixed to the energy resolution [Eq. (2)] used in the fit.

The dominant background source for the $\gamma\gamma e^+e^-$ final state is double radiative Bhabha scattering. For the $\gamma\gamma\mu^+\mu^-$ channel this background is expected to be substantially smaller. To obtain an estimate for these backgrounds we use our $\Upsilon(1S)$ sample (corresponding to an integrated luminosity of 32.5 pb^{-1}) subjected to the same set of cuts. Scaled to the size of our $\Upsilon(2S)$-sample, 4.5 candidates are found in the $e^+e^-\gamma\gamma$ channel and 1.1 candidates in the $\mu^+\mu^-\gamma\gamma$ channel.

Another background source is the $\pi\pi$ transition from the $\Upsilon(2S)$ to the $\Upsilon(1S)$[9]. In the transition $\Upsilon(2S) \to \pi^0\pi^0\Upsilon(1S)$, two photons from the π^0 decays may escape detection. Based on Monte Carlo simulations we find a contribution of less than 1 event. In addition, the charged pions from the $\Upsilon(2S) \to \pi^+\pi^-\Upsilon(1S)$ transition can be misidentified by the tube chambers and subsequently fake a photon shower pattern. The background due to this coincidence can be estimated from our measured $\pi^+\pi^-\Upsilon(1S)$ sample. Again a contribution of less than one event is found.

The contamination from the isospin violating transition $\Upsilon(2S) \to \pi^0\Upsilon(1S)$ is *a priori* expected to be negligible. Indeed, we find no events in our data sample with an effective mass in the π^0 mass region. Note that the SU_3 violating transition $\Upsilon(2S) \to \eta\Upsilon(1S)$ is kinematically excluded for events within the γ

energy range considered here.

Finally, the transition $\Upsilon(2S) \to \gamma\gamma\Upsilon(1S)$ can also receive a contribution from $\Upsilon(1S) \to \tau^+\tau^-$, when both τ's decay either into $e\nu\bar{\nu}$ or $\mu\nu\bar{\nu}$. Monte Carlo studies show that the expected number of events of this type is again less than one.

The sum of the estimated contributions from background sources evaluated above is compatible with the total number of background events listed in Table 1.

To determine $N_{res}[\Upsilon(2S)]$, the efficiency ϵ_{res} for detecting any $\Upsilon(2S)$ decay is calculated using the Lund Monte Carlo program[22]. We find $\epsilon_{res} = 0.86$ with an estimated systematic error of 0.07; the purely hadronic efficiency is greater than 90% but this value is reduced due to the presence of leptonic decay modes. Dividing the number of observed $\Upsilon(2S)$ decays (obtained by subtracting the continuum contribution from the total number of decays recorded in the detector) by ϵ_{res} we find $N_{res}[\Upsilon(2S)] = (201 \pm 16) \times 10^3$.

The efficiencies $\epsilon_J(\gamma\gamma l^+l^-)$ are evaluated using a Monte Carlo method. Samples of both $\gamma\gamma e^+e^-$ and $\gamma\gamma\mu^+\mu^-$ events are generated according to the assumed χ_b spin values J=2, 1, 0 taking into account all (E1 transition) angular correlations and the transverse beam polarization at the $\Upsilon(2S)$. The latter was measured with $e^+e^- \to \mu^+\mu^-$ and $e^+e^- \to \gamma\gamma$ events to be $(70 \pm 5)\%$. The generated particles are subjected to a simulated tracking through the Crystal Ball detector. The electromagnetic showers due to electrons and photons are simulated using the EGS program[23] while muon energy deposits are reproduced by using energy patterns from real $e^+e^- \to \mu^+\mu^-$ events. To simulate the DORIS machine background, we used "events" from a trigger which fires at every 10^7 beam crossing with no other condition. An "event" of this type is added onto each Monte Carlo event. The Monte Carlo samples thus obtained agree well with the measured data in basic aspects like energy patterns and background distributions. A software simulation of the trigger and the selection cuts described in section III are then applied to the Monte Carlo sample. Finally the charge tracking efficiency is incorporated. It is found to be 92% (per event) with an estimated systematic error of 4% using the final event sample from our $\Upsilon(2S) \to \pi^0\pi^0\Upsilon(1S) \to 4\gamma l^+l^-$

analysis[9]. This sample was obtained without using any chamber information and is practically background free. Table 4 lists the overall efficiencies obtained for all channels.

The branching ratios $\mathrm{BR}_J\left[\Upsilon(2S) \to \gamma\gamma e^+e^-\right]$ and $\mathrm{BR}_J\left[\Upsilon(2S) \to \gamma\gamma\mu^+\mu^-\right]$ for $J = 2$ and $J = 1$ are calculated using [Eq. (10)] with the values of N_J listed in Table 1, the backgrounds under the peaks obtained from the fits, the efficiencies ϵ_J listed in Table 4, and the number of resonance events N_{res} given above. The results are shown in Table 5. The systematic errors from the following sources are estimated: the Monte Carlo efficiency determination, the charge tracking efficiency, the fitting procedure, the number of produced $\Upsilon(2S)$ decays. In Table 6 we list the contribution of each source separately. These sub-errors are combined in quadrature to yield the final systematic error. Note that the branching ratios for the $\gamma\gamma e^+e^-$ and $\gamma\gamma\mu^+\mu^-$ channels are in good agreement. We then combine the results for both channels by taking the weighted averages,

$$\mathrm{BR}_2\left[\Upsilon(2S) \to \gamma\gamma l^+l^-\right] = (4.4 \pm 0.9 \pm 0.5) \cdot 10^{-4} \quad , \tag{11a}$$

$$\mathrm{BR}_1\left[\Upsilon(2S) \to \gamma\gamma l^+l^-\right] = (5.8 \pm 0.9 \pm 0.7) \cdot 10^{-4} \quad . \tag{11b}$$

To calculate an upper limit for the corresponding branching ratio of the χ_b^0 state, seen in the inclusive analysis at a photon transition energy of (163.8 ± 3.1) MeV, we allowed a third line in the fit to Fig. 7. Incorporating our resolution and our measured position of the third line, we obtain an upper limit of 3.7 events (90% C.L.). From this we calculate

$$\mathrm{BR}_0\left[\Upsilon(2S) \to \gamma\gamma l^+l^-\right] < 5 \times 10^{-5} \text{ (90\% C.L.)} \quad . \tag{11c}$$

Varying the spin assignments changes the efficiencies, and thus the branching ratios, by 10 to 15% at most.

Using an average branching ratio for $\Upsilon(1S) \to l^+l^-$ of (0.028 ± 0.003)[11] we can calculate from [Eq. (11)] the product branching ratios,

$$\mathrm{BR}_J \equiv \mathrm{BR}\left[\Upsilon(2S) \to \gamma\chi_b^J\right] \times \mathrm{BR}\left[\chi_b^J \to \gamma\Upsilon(1S)\right], \tag{12}$$

$$\begin{aligned} \mathrm{BR}_2 &= (1.6 \pm 0.3 \pm 0.2)\% \ , \\ \mathrm{BR}_1 &= (2.1 \pm 0.3 \pm 0.3)\% \ , \\ \mathrm{BR}_0 &< 0.2\% \ (90\% \ \mathrm{C.L.}) \ . \end{aligned} \tag{13}$$

The sum of the product branching ratios BR_J is also measured using the inclusive $\Upsilon(2S)$ photon spectrum[4]; it is given by the total branching ratio of the daughter lines in the 410–440 MeV region and found to be $(3.6 \pm 0.7 \pm 0.5)\%$, a value which agrees well with the sum of the branching ratios [Eq. (13)].

Part of the systematic error cancels in calculating the ratio $\mathrm{BR}_2/\mathrm{BR}_1$ of the χ_b^2 and χ_b^1 channels,

$$\frac{\mathrm{BR}_2}{\mathrm{BR}_1} = 0.76 \pm 0.19 \pm 0.06 \ . \tag{14}$$

Our results [Eqs. (13) and (14)] agree within errors with the corresponding CUSB measurements[3].

We can take our results one step further by using our inclusive branching ratios $\mathrm{BR}\left[\Upsilon(2S) \to \gamma\chi_b^J\right]$, $\left[(5.8 \pm 0.7 \pm 1.0)\% \text{ for } \chi_b^2, (6.5 \pm 0.7 \pm 1.2)\% \text{ for } \chi_b^1 \right.$ and $\left.(3.6 \pm 0.8 \pm 0.9)\% \text{ for } \chi_b^0 \ [4]\right]$ to calculate the branching ratios,

$$\begin{aligned} \mathrm{BR}\left[\chi_b^2 \to \gamma\Upsilon(1S)\right] &= (27 \pm 6 \pm 6)\% \ , \\ \mathrm{BR}\left[\chi_b^1 \to \gamma\Upsilon(1S)\right] &= (32 \pm 6 \pm 7)\% \ , \\ \mathrm{BR}\left[\chi_b^0 \to \gamma\Upsilon(1S)\right] &< \ \ 6\% \ (90\% \ \mathrm{C.L.}) \ . \end{aligned} \tag{15}$$

The systematic errors are evaluated by quadratically adding the systematic errors on the exclusive and inclusive branching ratios after leaving out the common uncertainty in $N_{res}\,[\Upsilon(2S)]$.

V. Hadronic Widths of χ_b States

The radiative branching ratios [Eq. (15)] are related to the hadronic widths of the χ_b states through the formula

$$\Gamma_{had}(\chi_b^J) = \Gamma_\gamma(\chi_b^J) \times \left[\frac{1}{\mathrm{BR}(\chi_b^J)} - 1\right] \ , \tag{16}$$

where $\Gamma_\gamma(\chi_b^J) \equiv \Gamma\left[\chi_b^J \to \gamma\Upsilon(1S)\right]$, and $\mathrm{BR}(\chi_b^J) \equiv \mathrm{BR}\left[\chi_b^J \to \gamma\Upsilon(1S)\right]$.

It has been argued that, especially for the $b\bar{b}$ system, $\Gamma_\gamma(\chi_b^J)$ is reliably estimated by an $E1$ transition[19],

$$\Gamma_\gamma(\chi_b^J) = \Gamma_{E1} = \frac{4}{9}\alpha e_q^2 k_J^3 \langle f \mid r \mid i\rangle^2 \quad , \tag{17}$$

where k is the photon momentum, e_q is the quark charge, $\alpha \sim 1/137$, and $\langle f \mid r \mid i\rangle$ is the dipole matrix element. This is because the $b\bar{b}$ system is considerably less relativistic than the lighter quark systems and corrections (including wave function distortions) are numerically much smaller. In addition the $1P \to 1S$ transition is free of the wave function "node" problem discussed in Ref. 19. In Table 7 we give $\Gamma_{E1}(\chi_b^J)$ calculated for various potential models; these models all give similar values.

The prediction of Ref. 17 is used in our estimate of the hadronic widths because this is the model which presently agrees best with our measurements of the COG and r for the χ_b^J states. It should be mentioned that this agreement might be a result of a particular choice of parameters rather than of the intrinsic accuracy of this model as compared to the others listed in Table 7.

From [Eq. (16)] we derive the hadronic widths $\Gamma_{had}^d(\chi_b^J)$,

$$\begin{aligned} \Gamma_{had}^d(\chi_b^2) &= (116 \pm 50)\ \mathrm{keV} \quad , \\ \Gamma_{had}^d(\chi_b^1) &= (77 \pm 32)\ \mathrm{keV} \quad , \\ \Gamma_{had}^d(\chi_b^0) &> 490\ \mathrm{keV}\ (90\%\ \mathrm{C.L.}) \quad , \end{aligned} \tag{18}$$

with the help of the theoretical prediction from Ref. 17. Using an average of all the predictions for $\Gamma_{E1}(\chi_b^J)$ in the table would change the values in Eq. (18) by about 10%. In [Eq. (18)], only the experimental statistical and systematic errors (added in quadrature) are taken into account.

The hadronic widths are calculated using QCD models[27], the calculation being more certain for the χ_b^2 and the χ_b^0 states than for the χ_b^1. Both the χ_b^2 and χ_b^0 can decay into two gluons, and one loop QCD corrections are available

(although renormalization scheme dependent). The χ_b^1 can decay into three gluons, but its leading annihilation contribution results from a singularity in the gluon — $q\bar{q}$ channel[27]; the first order correction for the χ_b^1 state has not yet been calculated.

The most model independent way to use the QCD-predictions is through their ratios. Since the matrix element is spin-independent[28], the wave function (at the origin) dependence cancels. Furthermore, the QCD-prediction for the ratio $\Gamma_{had}(\chi_b^2)/\Gamma_{had}(\chi_b^0)$ is, to first order in α_s, renormalization scheme independent[27]. For $\Gamma_{had}(\chi_b^1)/\Gamma_{had}(\chi_b^2)$, where only the lowest order prediction is available, the formula (see Table 8) was evaluated using a b-quark mass of 4.9 GeV and a confinement radius R_c of 1/400 MeV[24]. For both ratios we used the Mackenzie-Lepage scale [to make the first order QCD corrections for the hadronic Υ width vanish] and the resulting value for $\alpha_s = 0.165 \pm 0.005$[29][1].

As stated above, the QCD predictions for the absolute $\Gamma_{had}(\chi_b^J)$ are *a priori* less reliable because of the nature of the higher order QCD corrections needed. Nevertheless, there is interest in the absolute widths since in the case of charmonium the widths of the χ_c^J were significantly underestimated by theory[6,7,30]. Table 9 shows the comparison of our derived hadronic widths with the QCD predictions using the value of the derivative of the wave function at the origin from Ref. 17 and the $\overline{MS}$-renormalization scheme[31]. In contrast to the charmonium case, reasonable agreement between theory and experiment is observed. The calculation is, however, quite sensitive to the value of α_s used. Leaving α_s free while comparing the derived hadronic width of the χ_b^2 with its QCD-prediction, one finds,

$$\alpha_s^{exp} = 0.17 \pm 0.04 \quad , \tag{19}$$

where only the experimental errors have been taken into account.

VI. Conclusions

The production of two χ_b states is observed in the exclusive channel,

$$\Upsilon(2S) \to \gamma\chi_b,\ \chi_b \to \gamma\Upsilon(1S),\ \Upsilon(1S) \to e^+e^- \text{ or } \mu^+\mu^- \quad . \tag{20}$$

The observed photon energies agree within error with a previously reported Crystal Ball Collaboration inclusive measurement[4]. Combining these inclusive and exclusive measurements new values are derived for the χ_b^2, χ_b^1 masses,

$$\begin{aligned} M_2 &= (9914.6 \pm 1.6)\ \text{MeV} \quad , \\ M_1 &= (9891.1 \pm 1.5)\ \text{MeV} \quad , \end{aligned} \tag{21}$$

the Center of Gravity of the 1^3P_J states,

$$M\left[\chi_b^{cog}\right] = (9900.5 \pm 1.3)\ \text{MeV} \quad , \tag{22}$$

and the fine structure splitting parameter, $r = [M_2 - M_1]\,/\,[M_1 - M_0]$,

$$r = 0.71 \pm 0.08 \quad , \tag{23}$$

where the COG and r are obtained also using our previously reported inclusive measurement of the $J = 0$ line .[4]

Branching ratios are determined for the cascade of [Eq. (20)] yielding,

$$\begin{aligned} &\text{BR}\left[\Upsilon(2S) \to \gamma\chi_b^2\right] \times \text{BR}\left[\chi_b^2 \to \gamma\Upsilon(1S)\right] = (1.6 \pm 0.3 \pm 0.2)\% \quad , \\ &\text{BR}\left[\Upsilon(2S) \to \gamma\chi_b^1\right] \times \text{BR}\left[\chi_b^1 \to \gamma\Upsilon(1S)\right] = (2.1 \pm 0.3 \pm 0.3)\% \quad , \\ &\text{BR}\left[\Upsilon(2S) \to \gamma\chi_b^0\right] \times \text{BR}\left[\chi_b^0 \to \gamma\Upsilon(1S)\right] < 0.2\%\ (90\%\ C.L.) \quad . \end{aligned} \tag{24}$$

Again, using our previously reported inclusive measurements and the values of [Eq. (24)], we find,

$$\begin{aligned} &\text{BR}\left[\chi_b^2 \to \gamma\Upsilon(1S)\right] = (27 \pm 6 \pm 6)\% \quad , \\ &\text{BR}\left[\chi_b^1 \to \gamma\Upsilon(1S)\right] = (32 \pm 6 \pm 7)\% \quad , \\ &\text{BR}\left[\chi_b^0 \to \gamma\Upsilon(1S)\right] < 6\%(90\%C.L.) \quad . \end{aligned} \tag{25}$$

By using theoretical estimates for the (total) radiative widths of the χ_b^1, χ_b^2 states, the hadronic widths of these states are derived and the resulting widths are then compared with QCD models. In contrast to the case of charmonium, there is reasonable agreement between the experimental values and corresponding theoretical predictions. The presently available data should allow reduction of the uncertainty in the assumptions and parameters for quarkonium models.

Acknowledgements

This experiment would not have been possible without the dedication of the DORIS machine group as well as the experimental support groups at DESY. We would like to thank the DESY and SLAC directorate for their support. We acknowledge useful discussions with H. Janssen and M. Peskin on the subject of Section V. Some of us (Z.J., B.N., and G.N.) thank DESY for financial support. D.W. acknowledges financial support from the National Science Foundation. E.D.B., R.H., and K.S. have benefitted from financial support from the Humboldt Foundation. The Nijmegen group acknowledges the support of FOM-ZWO. The Erlangen, Hamburg, and Würzburg groups acknowledge financial support from the Bundesministerium fur Forschung and Technologie and the Deutsche Forschungsgemeinschaft (Hamburg). This work was supported in part by the U.S. Department of Energy under Contract No. DE-AC03-81ER40050 (CIT), No. DE-AC02-76ER03066 (CMU), No. DE-AC02-76ER03064 (Harvard), No. DE-AC02-76ER03072 (Princeton), No. DE-AC03-76SF00515 (SLAC), No. DE-AC03-76SF00326 (Stanford), and by the National Science Foundation under Grants No. PHY75-22980 (CIT), No. PHY81-07396 (HEPL), No. PHY82-08761 (Princeton).

References

♯ Present Address: Institute for Particle Physics, University of California, Santa Cruz, California 95064, USA.

† Permanent Address: DPHPE, Centre d'Etudes Nucléaires de Saclay, Gif sur Yvette, France.

⋆ Present Address: Department of Physics, Princeton University, Princeton, NJ 08544 USA.

• Present Address: KEK Tsukuba National Lab for High Energy Physics, Oho-Machi, Tsukuba, Japan (Kin) 300-32.

% Permanent Address: Cracow Institute of Nuclear Physics, Cracow, Poland.

‡ Present Address: Fermilab, MS-223, P.O. Box 500, Batavia, IL 60510.

◇ Present Address: Vanderbilt University, Nashville, TN 37203 USA.

‡ Present Address: Nuclear Physics Laboratory, Oxford University, Keble Roiad OX1 3RH, England.

♭ Present Address: Department of Physics, University of Wisconsin, Madison, WI 53706.

⇕ Present Address: CERN, 1211 Geneva 23, Switzerland.

1. See for example W. Buchmüller, CERN-TH 3938/84, to be published in Proceedings of the International School of Physics of Exotic Atoms, Erice, 1984.

2. C. Klopfenstein *et al.* (CUSB), Phys. Rev. Lett. **51**, 160 (1983); P. Haas *et al.* (CLEO), Phys. Rev. Lett. **52**, 799 (1984).

3. F. Pauss *et al.* (CUSB), Phys. Lett. **130B**, 439 (1983). For revised results on the branching ratios see: J. Lee-Franzini (CUSB), invited talk at the 5th International Conference on: Physics in Collision, Autun, France, July 3–5, 1985.

4. R. Nernst *et al.* (Crystal Ball), Phys. Rev. Lett. **54**, 2195 (1985).

5. H. Albrecht *et al.* (ARGUS), Phys. Lett. **160B**, 331 (1985).

6. E. Bloom and C. Peck, Ann. Rev. Nucl. Part. Sci. **33**, 143 (1983); M. Oreglia *et al.* (Crystal Ball), Phys. Rev. **D25**, 2259 (1982); M. Oreglia, Ph.D. Thesis, Stanford Univ., SLAC-226, unpublished (1980).

7. J. Gaiser, Ph.D. Thesis, Stanford Univ., SLAC-255, unpublished (1985).

8. R. Lee, Ph.D. Thesis, Stanford Univ., SLAC-282, unpublished (1985).

9. D. Gelphman *et al.* (Crystal Ball), Phys. Rev. **D32**, 2893 (1985).

10. The mass difference $\Delta M = M[\Upsilon(2S)] - M[\Upsilon(1S)] = (563.2 \pm 0.6)$ MeV has been measured precisely using the resonance depolarisation technique: A. Artamonov *et al.*, Phys. Lett. **118B**, 225 (1982); D. Barber *et al.*, Phys. Lett. **135B**, 498 (1984).

11. Rev. Mod. Phys. **56**, nr. 2, Part II (Particle Data Book), April 1984.

12. T. Skwarnicki (Crystal Ball), in the Proceedings of the XXth Rencontre de Moriond, p. 291, Les Arcs-Savoie, France, March 10–17, 1985, edited by J. Tran Thanh Van (Edtions Frontieres, Singapore, 1985).

13. R. Barbieri, R. Gatto and R. Kögerler, Phys. Lett. **60B**, 183, (1976).

14. M. Bander, B. Klima, U. Maor and D. Silverman, Phys. Lett. **134B**, 258 (1984).

15. W. Buchmüller, Phys. Lett. **112B**, 479 (1982).

16. E. Eichten and F. Feinberg, Phys. Rev. **D23**, 2724 (1981); D. Gromes, Z. Phys. **C26**, 401 (1984).

17. S. Gupta, S. Radford and W. Repko, Preprint WSU-Th, August 1985.

18. A. Martin, Phys. Lett. **100B**, 511 (1981).

19. R. McClary and N. Byers, Phys. Rev. **D28**, 1692 (1983).

20. P. Moxhay and J. Rosner, Phys. Rev. **D28**, 1132 (1983).

21. K. Hagiwara, S. Jacobs, M. Olsson and K. Miller, Phys. Lett. **131B**, 455 (1983).

22. B. Anderson *et al.*, Phys. Rep. **97**, 33 (1983).

23. R. Ford and W. Nelson, SLAC-210 (1978).

24. W. Buchmüller and S. Tye, Phys. Rev. **D24**, 132 (1981).

25. E. Eichten, K. Gottfried, K. Lane and T. Yan, Phys. Rev. **D21**, 203 (1980).

26. M. Olsson, A. Martin and A. Peacock, Phys. Rev. **D31**, 81 (1985).

27. R. Barbieri, R. Gatto and E. Remiddi, Phys. Lett. **61B**, 465 (1976); R. Barbieri, M. Caffo, R. Gatto and E. Remiddi, Phys. Lett. **95B**, 93 (1980); R. Barbieri, M. Caffo, R. Gatto and E. Remiddi, Nucl. Phys. **B192**, 61 (1981); R. Barbieri, R. Gatto and E. Remiddi, Phys. Lett. **106B**, 497 (1981).

28. In fact only for the Moxhay-Rosner potential a spin dependence of a few percent is found (see Ref. 20).

29. P. Mackenzie and G. Lepage, Phys. Rev. Lett. **47**, 1244 (1981).

30. This has been attributed to wave function corrections or to an abnormally large α_S of at least 0.4. The latter possibility is not very attractive since the ratio $\Gamma_{had}(\chi_c^2)/\Gamma_{had}(\chi_c^0)$, which depends rather strongly on α_S but in which wave function distortions cancel, is predicted correctly using $\alpha_S \approx 0.2$ (see Ref. 26 for a discussion on this point). As noted, wave function corrections are expected to be small in the case of bottomonium.

31. For the calculation of these predictions we used the scale $\mu = 0.48\, M_\Upsilon$ to remain consistent with the Mackenzie-Lepage value for α_s adopted before[29]. The values for m_b and R_c are chosen as before. There also appears a term inversely proportional to the relative quark velocity; this term becomes divergent in the zero binding-energy limit. We assumed this term to be absorbed in the wave function.

Table 1. The results of the fits (see text) to the final cascade samples as illustrated in Fig. 7. Only statistical errors are given.

	$\gamma\gamma\mu^+\mu^-$	$\gamma\gamma e^+e^-$	$\gamma\gamma l^+l^-$
E_2 (MeV)	$108.3^{+1.9}_{-1.8}$	106.0 ± 1.4	107.0 ± 1.1
E_1 (MeV)	131.7 ± 1.4	131.8 ± 1.3	131.7 ± 0.9
N_2	$15.5^{+4.7}_{-4.1}$	$19.6^{+5.1}_{-4.4}$	$34.7^{+6.8}_{-6.1}$
N_1	$22.8^{+5.5}_{-4.8}$	$29.8^{+6.1}_{-5.4}$	$52.9^{+8.1}_{-7.4}$
Background from fit[a]	$1.4^{+1.2}_{-0.7}$	$1.4^{+1.2}_{-0.8}$	$2.8^{+1.6}_{-1.2}$
Background from side bands[b]	1.1 ± 1.1	3.8 ± 2.0	4.9 ± 2.2

[a] Integrated over the range 93 MeV $\leq E_{\gamma low} \leq$ 148 MeV $(E_2 - 3\sigma_2, E_1 + 3\sigma_1)$, where $\sigma_{1,2}$ refer to the resolution on the photon energy at $E_{1,2}$.

[b] See Fig. 5. Estimated by scaling down to the energy interval considered here, the total number of entries in the two (3σ wide) ΔM regions left and right of the (6σ wide) central ΔM region (σ refers to the resolution on ΔM).

Table 2. Contributions to the systematic error ΔE_J in the values of the energies E_2 and E_1.

Source of uncertainty	ΔE_2 (MeV)	ΔE_1 (MeV)
1 Energy scale	.5	.5
2 Event selection	.5	.5
3 Fitting procedure	.3	.3
Final error(a)	1.3	1.3

[a] Linear sum of sub-errors 1, 2, and 3 (see main text).

Table 3. Comparison of experimental values for r and the position of the center of gravity (see text) with predictions from a range of potential models.

Source	r	$M\left[\chi_b^{cog}\right]$ (MeV)
This experiment	0.71 ± 0.08	9900.5 ± 1.3
Bander-Klima-Maor-Silverman[14]	0.77	9891
Buchmüller[15]	0.76	9889[a]
Eichten-Feinberg-Gromes[16]	0.80	9927[b]
Gupta-Radford-Repko[17]	0.68	9901
Martin[18]	–	9861
McClary-Byers[19]	0.45	9925
Moxhay-Rosner[20]	0.42	9906
Wisconsin[21]	–	9894

[a] The input value for $M\left[\Upsilon(1S)\right]$ used in this model has been scaled up by 27 MeV to 9460 MeV.

[b] The input value for $M\left[\Upsilon(2S)\right]$ used in this model has been scaled up by 3 MeV to 10023 MeV.

Table 4. Overall efficiencies determined as described in the text. Only statistical errors are given.

$\epsilon(\gamma\gamma e^+e^-)$		$\epsilon(\gamma\gamma\mu^+\mu^-)$	
Assuming $J=0$	$.206 \pm .008$	Assuming $J=0$	$.170 \pm .008$
Assuming $J=1$	$.256 \pm .009$	Assuming $J=1$	$.196 \pm .009$
Assuming $J=2$	$.218 \pm .008$	Assuming $J=2$	$.179 \pm .008$

Table 5. Product branching ratios $\mathrm{BR}_J\left[\Upsilon(2S) \to \gamma\gamma l^+l^-\right]$ as defined in the text.

$\mathrm{BR}_2\left[\Upsilon(2S) \to \gamma\gamma e^+e^-\right]$	$(4.5^{+1.2}_{-1.0} \pm 0.5) \cdot 10^{-4}$
$\mathrm{BR}_1\left[\Upsilon(2S) \to \gamma\gamma e^+e^-\right]$	$(5.8^{+1.2}_{-1.1} \pm 0.7) \cdot 10^{-4}$
$\mathrm{BR}_2\left[\Upsilon(2S) \to \gamma\gamma \mu^+\mu^-\right]$	$(4.3^{+1.3}_{-1.2} \pm 0.5) \cdot 10^{-4}$
$\mathrm{BR}_1\left[\Upsilon(2S) \to \gamma\gamma \mu^+\mu^-\right]$	$(5.8^{+1.4}_{-1.3} \pm 0.7) \cdot 10^{-4}$

Table 6. Contributions to the systematic errors on the product branching ratios $\mathrm{BR}_J\left[\Upsilon(2S) \to \gamma\gamma l^+l^-\right]$.

Source of uncertainty	muon channel via (χ_b^2)	muon channel via (χ_b^1)	electron channel via (χ_b^2)	electron channel via (χ_b^1)
1. Monte Carlo efficiency	7%	7%	6%	6%
2. Charged tracking efficiency	4%	4%	4%	4%
3. Fitting procedure	4%	3%	4%	3%
4. $N_{res}\left[\Upsilon(2S)\right]$	8%	8%	8%	8%
Final error[(a)]	12.0%	11.7%	11.5%	11.2%

(a) Computed by combining the sub-errors 1 through 4 in quadrature.

Table 7. Theoretical widths for the E1 transitions $\chi_b^J \rightarrow \gamma\Upsilon(1S)$, calculated using $\Gamma_{E1} = \frac{4}{9}\alpha e_q^2 k_J^3 \langle f \mid r \mid i\rangle^2$, with $\langle f \mid r \mid i\rangle$ from the listed references and taking the photon energies observed in this experiment. Also listed is $\mid R'_p(0) \mid^2$ (see text).

Potential	$\langle f \mid r \mid i\rangle^2$ $(\mathrm{GeV})^{-2}$	$\Gamma_{E1}(\chi_b^2)$ keV	$\Gamma_{E1}(\chi_b^1)$ keV	$\Gamma_{E1}(\chi_b^0)$ keV	$\mid R'_p(0) \mid^2$ $(\mathrm{GeV})^5$
Buchmüller-Tye [24]	1.26	40	34	27	1.42[a]
Cornell [25][b]	1.14	36	31	24	1.39
Gupta-Radford-Repko[17]	1.35	43	36	29	1.56[a]
Martin[18][b]	1.37	43	37	29	1.34
McClary-Byers[19]	1.02	33	28	22	1.96[a]
Moxhay-Rosner[20]	1.24[c]	39	34	27	1.53[a]
Wisconsin[21][b]	1.28	40	35	27	1.44

(*a*) From private communication with the author(s).

(*b*) The numerical values for $\langle f \mid r \mid i\rangle$ and $\mid R'_p(0) \mid^2$ are taken from Ref. 20.

(*c*) The value for $\langle f \mid r \mid i\rangle$ corresponds to the spin-averaged result. The small spin-dependent corrections which are found, lead to changes for Γ_{E1} of less than 1 keV.

Table 8. Experimental ratios of hadronic widths for the χ_b states and the QCD prediction[a] to lowest and first order, calculated according to the method described in the text.

Ratio	This experiment[b]	QCD[0]	QCD[1]
$\frac{\Gamma_{had}(\chi_b^0)}{\Gamma_{had}(\chi_b^2)}$	> 3.8 (90% C.L.)	$\frac{15}{4}$ $= 3.75$	$\frac{15}{4} \cdot (1 + 9.5\frac{\alpha_s}{\pi})$ $= 5.6 \pm 0.1$
$\frac{\Gamma_{had}(\chi_b^1)}{\Gamma_{had}(\chi_b^2)}$	0.68 ± 0.30	$\frac{20}{9\pi}\,\alpha_s \ln(m_b R_c)$ $= 0.29 \pm 0.01$	not known

(*a*) In the error on the QCD predictions, only the error on α_s was taken into account.

(*b*) The errors on the experimental values were obtained by adding the statistical and systematic errors in quadrature, leaving out the common systematic effects which cancel in the ratio.

Table 9. Comparison of the derived hadronic widths (in keV) for the χ_b states and the QCD prediction [a] to lowest and first order (in the $\overline{MS}$-scheme), calculated according to the method described in the text.

State	Derived Width	QCD$^{(0)}$	QCD$^{(1)}$
χ_b^2	116 ± 50	$\frac{128}{5}\alpha_s^2 \frac{\mid R'_p(0) \mid^2}{M^4}$ $= 113 \pm 7$	$\text{QCD}^{(0)} \cdot (1 + 0.3\frac{\alpha_s}{\pi})$ $= 115 \pm 7$
χ_b^1	77 ± 32	$\frac{512}{9\pi}\alpha_s^3 \frac{\mid R'_p(0) \mid^2}{M^4} \ln(m_b R_c)$ $= 33 \pm 3$	not known
χ_b^0	> 490 (90% C.L.)	$96\alpha_s^2 \frac{\mid R'_p(0) \mid^2}{M^4}$ $= 424 \pm 26$	$\text{QCD}^{(0)} \cdot (1 + 9.8\frac{\alpha_s}{\pi})$ $= 643 \pm 46$

[a] In calculating the errors on the QCD predictions, only the error on α_s was taken into account.

Figure Captions

Fig. 1. The energy level scheme for $b\bar{b}$ bound states that can be reached by a radiative transition from the $\Upsilon(2S)$. The solid lines represent the observed transitions.

Fig. 2. Schematic of the detector as configured at DESY for this experiment.

Fig. 3. Event map for $\Upsilon(2S) \rightarrow \gamma\gamma\mu^+\mu^-$ event. The energy is given in MeV for all crystals containing more than 0.5 MeV.

Fig. 4. Event map for $\Upsilon(2S) \rightarrow \gamma\gamma e^+e^-$ event. The energy is given in MeV for all crystals containing more than 0.5 MeV.

Fig. 5. Scatter plot of the lowest of the two photon energies vs. the mass difference $\Delta M = [\Upsilon(2S)] - M\left(l^+l^-\right)$ for all 282 events surviving the selection cuts for the $\gamma\gamma l^+l^-$ final state (see text). The horizontal lines indicate the side-bands: 3σ wide regions on both sides of the 6σ wide signal band. The arrows indicate the final cut on ΔM.

Fig. 6. Projection of Fig. 5 on the ΔM-axis for 440 MeV $< \Delta M <$ 680 MeV. The curve represents the fit to a NaI-line shape on top of a flat background (see text).

Fig. 7. Projection of the signal band (100 events) in Fig. 5 on the $E_{\gamma\text{low}}$ axis. The curve represents the fit to two NaI-line shapes of fixed width on top of a flat background (see text).

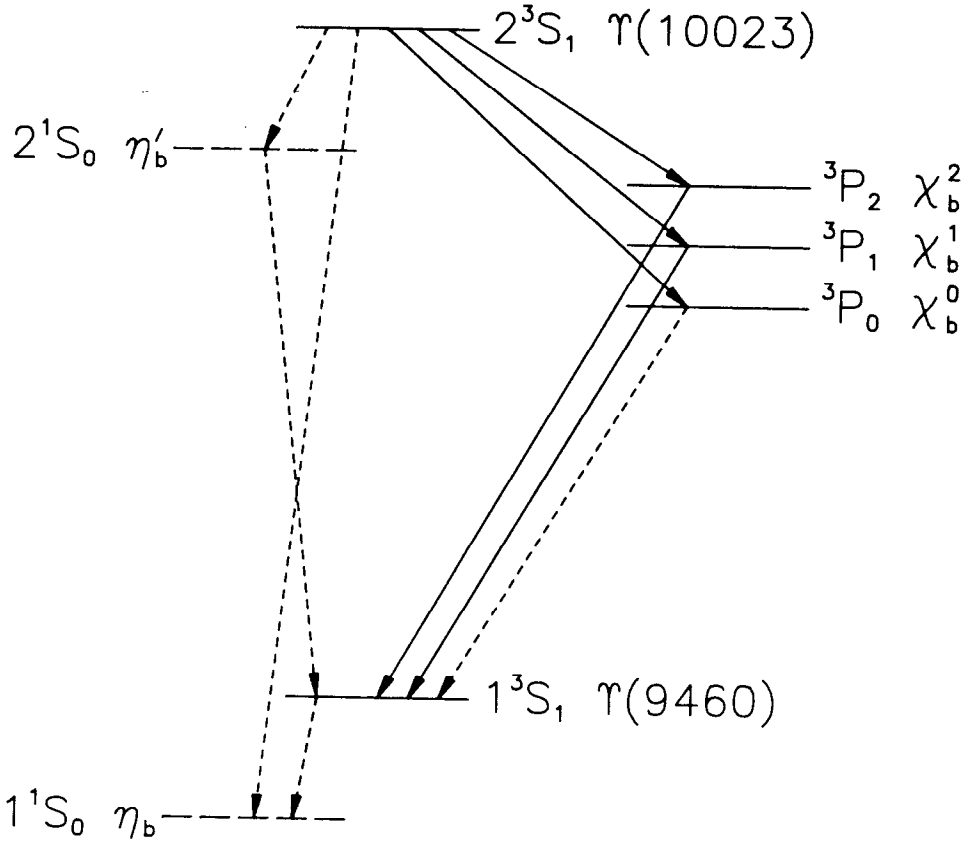
2^3S_1 $\Upsilon(10023)$
2^1S_0 η_b'
$^3P_2$ χ_b^2
$^3P_1$ χ_b^1
$^3P_0$ χ_b^0
1^3S_1 $\Upsilon(9460)$
1^1S_0 η_b

Fig. 1

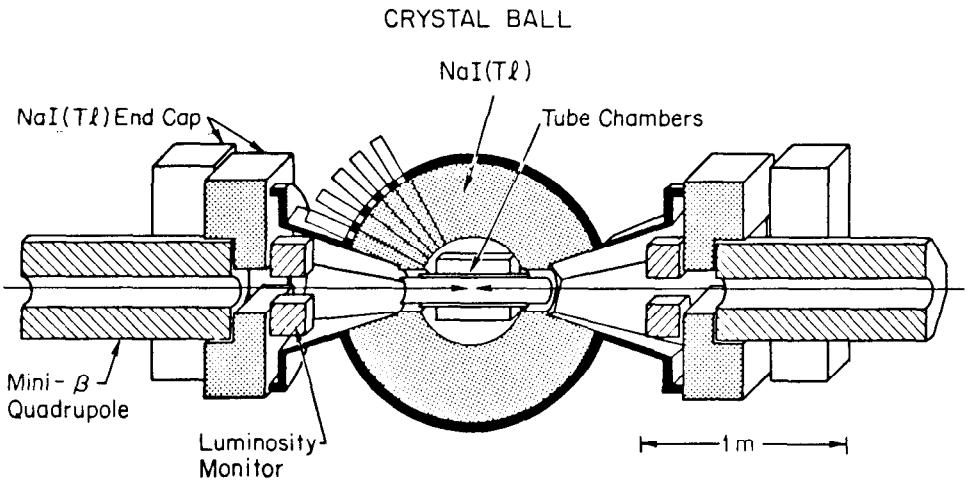
CRYSTAL BALL
NaI(Tℓ)
NaI(Tℓ) End Cap
Tube Chambers
Mini-β
Quadrupole
Luminosity
Monitor
1 m

Fig. 2

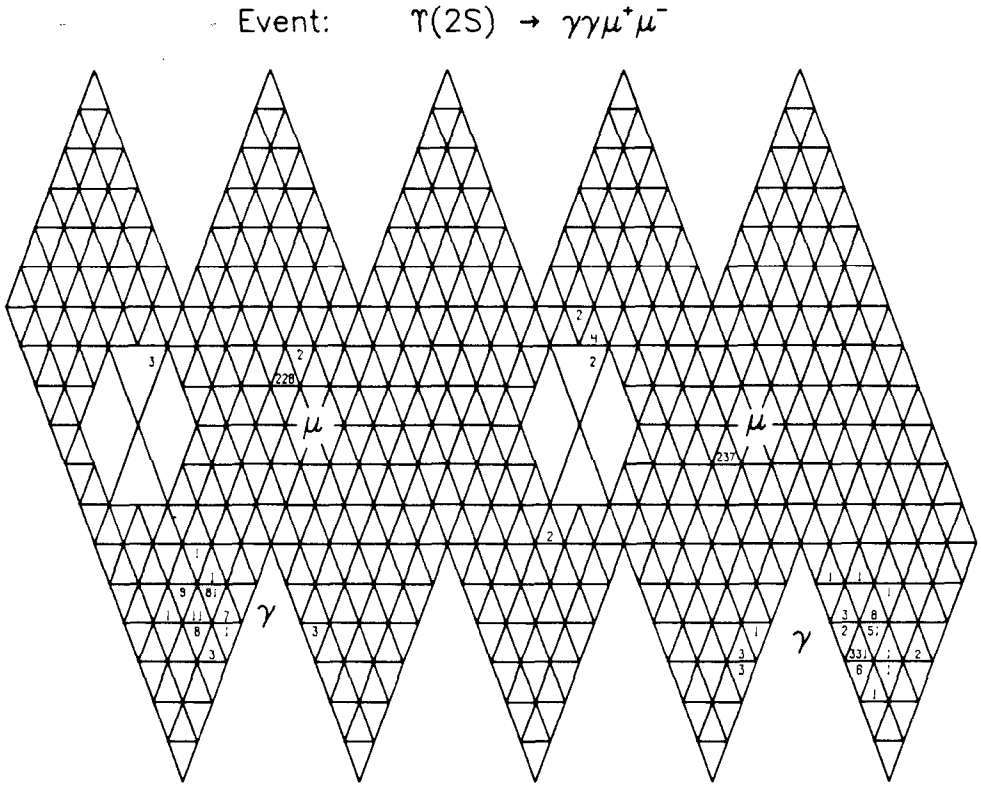
Event: $\Upsilon(2S) \rightarrow \gamma\gamma\mu^+\mu^-$
μ
μ
γ
γ

Fig. 3

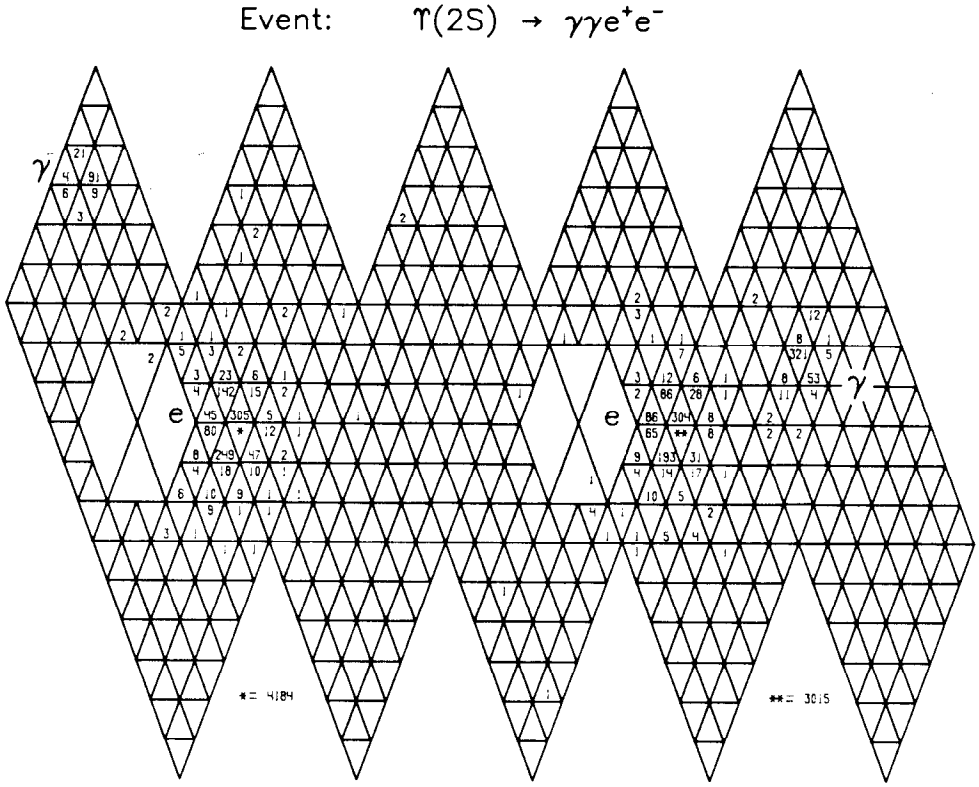
Event: $\Upsilon(2S) \rightarrow \gamma\gamma e^+e^-$
γ
e
e
γ
*= 4184
**= 3015

Fig. 4

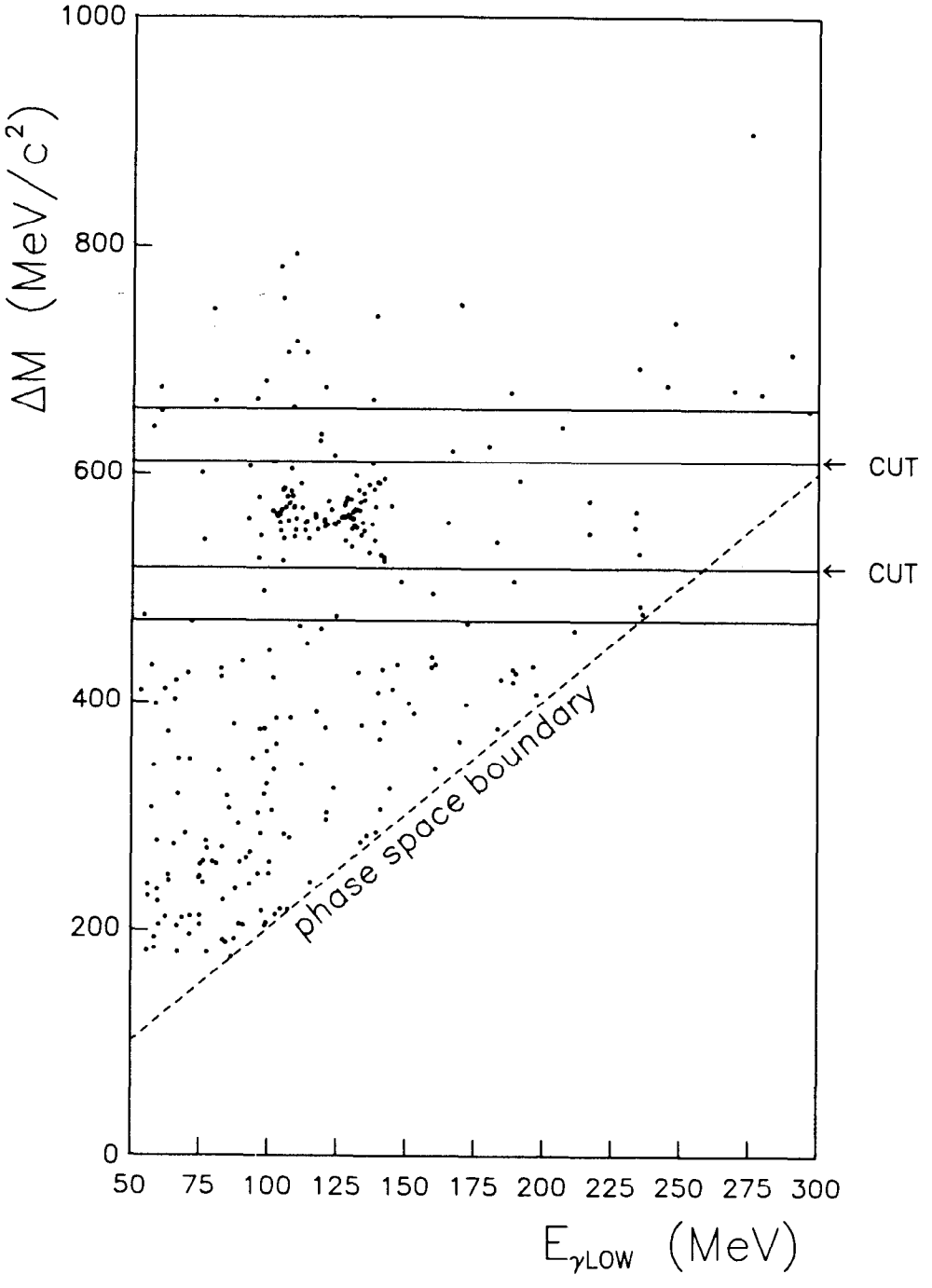
1000
800
600
400
200
0
ΔM (MeV/c²)
CUT
CUT
phase space boundary
50 75 100 125 150 175 200 225 250 275 300
Eγ LOW (MeV)

Fig. 5

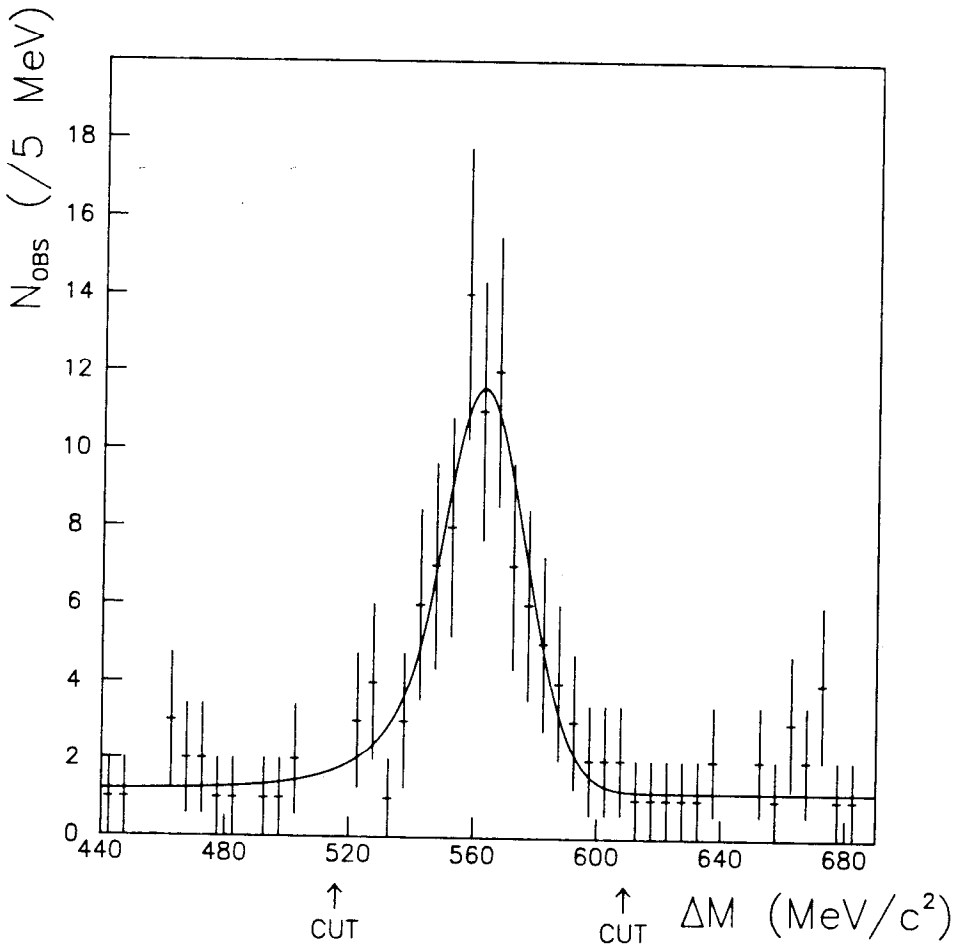
N_{OBS} (/5 MeV)
18
16
14
12
10
8
6
4
2
0
440
480
520
560
600
640
680
CUT
CUT
ΔM (MeV/c²)

Fig. 6

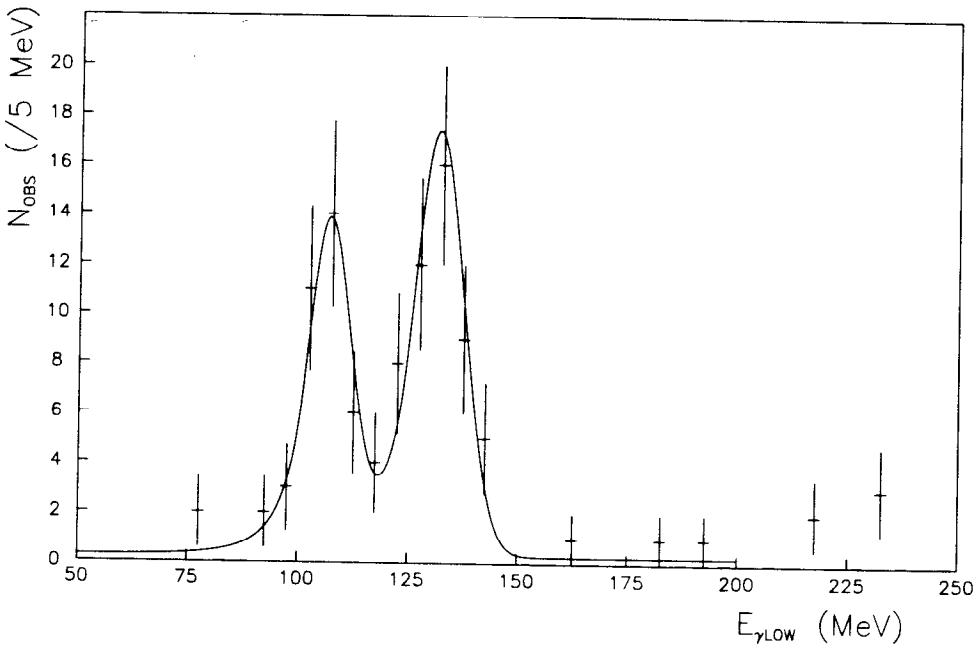
N_{OBS} (/5 MeV)
0
2
4
6
8
10
12
14
16
18
20
50
75
100
125
150
175
200
225
250
$E_{\gamma LOW}$ (MeV)

Fig. 7